ACADEMIC PRESS

Available online at www.sciencedirect.com
SCIENCE DIRECT®

Journal of Catalysis 219 (2003) 176–185

JOURNAL OF CATALYSIS

www.elsevier.com/locate/jcat

Structural change of Ni species during the methane decomposition and the subsequent gasification of deposited carbon with CO_2 over supported Ni catalysts

Sakae Takenaka,* Emi Kato, Yo Tomikubo, and Kiyoshi Otsuka

Department of Applied Chemistry, Graduate School of Science and Engineering, Tokyo Institute of Technology, Ookayama, Meguro-ku, Tokyo 152-8552, Japan

Received 13 December 2002; revised 21 March 2003; accepted 3 April 2003

Abstract

The structural changes of Ni species in Ni/Al_2O_3, Ni/SiO_2, and Ni/TiO_2 catalysts during the repeated cycles of the methane decomposition and the subsequent gasification of deposited carbons with CO_2 have been studied. The catalytic activity for the methane decomposition depended on the size of Ni metal particles; i.e., the particle size from 60 to 100 nm was most effective. The catalytically active Ni species in Ni/SiO_2 were present as Ni metal particles with diameter from 40 to 100 nm at the first reaction cycle, but they were aggregated into ones with diameters larger than 200 nm, resulting in the deactivation of Ni/SiO_2 for methane decomposition. In contrast, catalytic activity of Ni/TiO_2 was kept high during the repeated reactions because the particle size of Ni metal was kept at the optimum size range effective for the methane decomposition. On the other hand, Ni species in a fresh Ni/Al_2O_3 were composed of highly dispersed Ni(II) species and Ni metal particles of a diameter smaller than 20 nm. During the repeated reactions, the Ni(II) species were gradually reduced, forming the fine Ni metal particles, and the fine metal particles were aggregated into ones with a larger diameter, which brought about an increase in the catalytic activity of Ni/Al_2O_3.

Keywords: Ni/Al_2O_3; Ni/SiO_2; Ni/TiO_2; CH_4 decomposition; Gasification of carbon nanofiber; Particle size of Ni metal

1. Introduction

The increase in CO_2 concentration in the atmosphere due to increasing burning of fossil fuels (petroleum, coal, and natural gas) may lead to irreversible disastrous changes in the climate of our planet. Hydrogen is a clean-burning, nonpolluting fuel that can eliminate many of our insufferable environmental, economic, and health problems. In the near future, hydrogen would be utilized widely as a fuel for H_2–O_2 fuel cells. However, the current processes of hydrogen production use fossil fuels and water, emitting huge quantities of CO_2 into the atmosphere. In addition, hydrogen inevitably contains CO, which poisons strongly the Pt electrocatalysts at the anode of fuel cells. Therefore, a new method for hydrogen synthesis without production of CO and CO_2 is required.

Methane decomposition into hydrogen and carbon is of current interest as an alternative route of hydrogen synthesis because the reaction does not produce CO_2 nor CO [1,2]. Supported Ni catalysts are well known as being effective for methane decomposition into hydrogen and carbon nanofibers [3–7]. Only hydrogen is produced as a gaseous product in methane decomposition over supported Ni catalysts. Thus, hydrogen can be supplied directly to fuel cells. However, the catalytic activity of supported Ni catalysts for methane decomposition decreases with time on stream and finally the catalysts are deactivated completely due to the deposition of graphite layers onto the surface of Ni metal [8]. To supply hydrogen successively through methane decomposition to fuel cells, catalysts deactivated for the methane decomposition should be regenerated by removal of carbons. In a previous paper, we demonstrated that the treatment of the deactivated catalysts in a flow of CO_2 at 923 K resulted in the recovery of catalytic activity for methane decomposition as well as production of CO due to the gasification of deposited carbons with a conversion higher than 95%

* Corresponding author.
E-mail address: stakenak@o.cc.titech.ac.jp (S. Takenaka).

0021-9517/$ – see front matter
doi:10.1016/S0021-9517(03)00152-0

($C + CO_2 \rightarrow 2CO$) [9]. These results suggest that the production of hydrogen for fuel cells and that of CO as a synthetic reagent for the chemical industry can be performed repeatedly without CO_2 emission. The conversion of deposited carbons into CO was always higher than 95% irrespective of the number of repeated cycles and of the type of catalytic supports of Ni [10]. However, the catalytic activity for methane decomposition decreased or increased with the repeated reactions according to the type of catalytic supports; i.e., Ni/SiO_2 showed high activity in the early cycles but the activity decreased with repeated cycles, whereas the catalytic activity of Ni/TiO_2 was kept high and that of Ni/Al_2O_3 increased with the repeated reactions. We speculate that the change in the catalytic activity for methane decomposition results from the structural changes of Ni species during the repeated reactions.

The purpose in this work is to examine the structural changes of Ni species in supported Ni catalysts (Ni/Al_2O_3, Ni/SiO_2, and Ni/TiO_2) during the repeated cycles of methane decomposition and subsequent gasification of carbon nanofibers with CO_2 by Ni K-edge XAFS (XANES/EXAFS), XRD, scanning electron microscopy (SEM), and back-scattering electron microscopy. The role of catalytic supports in the structural changes of Ni species will be discussed on the basis of these spectroscopic studies.

2. Experimental

Supported Ni catalysts were prepared by impregnation of the supports (Al_2O_3, SiO_2, and TiO_2) with an aqueous solution of $Ni(NO_3)_2 \cdot 6H_2O$, followed by drying up of the impregnated samples at 373 K in air. The samples were calcined at 873 K for 5 h in air. Al_2O_3 (JRC-ALO4; 177 $m^2\,g^{-1}$), SiO_2 (Cab-O-Sil supplied from Cabot. Co.; 200 $m^2\,g^{-1}$), and TiO_2 (JRC-TIO4; 50 $m^2\,g^{-1}$) were utilized as catalytic supports of Ni. The JRC-ALO4 and JRC-TIO4 were supplied as reference catalysts from the Catalysis Society of Japan. Methane decomposition over the supported Ni catalysts was carried out in a conventional gas-flow system. Prior to the reaction, the Ni catalyst was treated in a stream of hydrogen at 873 K for 1 h. The methane decomposition was initiated by contact of methane with the reduced catalyst at 823 K. After the catalyst was deactivated completely for methane decomposition, the methane remaining in the reactor was purged out with an Ar stream at 823 K and the temperature was raised to 923 K. Gasification of the deposited carbon was followed by introduction of CO_2 into the same reactor at 923 K. During methane decomposition and gasification of deposited carbons, a part of the gases in the exit stream from the catalyst bed was sampled out and analyzed by on-line gas chromatography. In this study, Ni (5 wt%)/Al_2O_3, Ni (5 wt%)/SiO_2, and Ni (2.5 wt%)/TiO_2 were utilized unless otherwise noted because these catalysts suggested the typical effects of catalytic supports on the catalytic activity changes during the repeated reactions [10], as will be described in more detail in the Results and discussion section in this paper. In the present study, the amount of carbons deposited on the catalysts by methane decomposition and of those converted into CO by gasification with CO_2 were estimated from the total amounts of hydrogen and CO formed during the reactions, respectively, assuming that the reactions, $CH_4 \rightarrow C + 2H_2$ and $C + CO_2 \rightarrow 2CO$, occurred selectively. In fact, formation of only H_2 and only CO could be observed during methane decomposition and gasification of deposited carbons with CO_2, respectively.

SEM images and back-scattering electron images of the catalyst were measured using a Hitachi FE-SEM S-800 (field emission gun scanning electron microscope).

X-ray absorption experiments were carried out on the beam line BL-9A at the Photon Factory in the Institute of Materials Structure Science for High Energy Accelerator Research Organization, Tsukuba, Japan, with a ring energy of 2.5 GeV and a stored current of 250–450 mA (Proposal No. 2002G255). The X-ray absorption spectra of Ni/Al_2O_3, Ni/SiO_2, and Ni/TiO_2 were recorded in a fluorescence mode with a Si(111) two-crystal monochromator at room temperature. The X-ray absorption spectra of Ni foil and NiO were recorded in a transmission mode at room temperature. Normalization of XANES and analyses of EXAFS were performed as described elsewhere [11].

X-ray diffraction (XRD) patterns were measured by a Rigaku RINT 2500V difractometer using Cu-K_α radiation at room temperature.

To prepare the catalyst sample for the measurement of Ni K-edge XAFS, XRD, SEM images, and back-scattering electron images, methane decomposition at 823 K and subsequent gasification of deposited carbons with CO_2 at 923 K were performed repeatedly over the catalyst. For the purpose of the structural analysis of Ni species in the catalyst, methane decomposition was ceased in the early period, where moles of carbons deposited per mole of the total Ni atoms in the catalysts (C/Ni) were 20–50. The structure of Ni species in the catalyst which had been deactivated completely for methane decomposition was also examined.

3. Results and discussion

3.1. Reaction cycles for supported Ni catalysts

Methane decomposition at 823 K and subsequent gasification of deposited carbon with CO_2 at 923 K were examined repeatedly for Ni/Al_2O_3, Ni/SiO_2, and Ni/TiO_2 [10]. Fig. 1 shows the changes in the formation rate of hydrogen in methane decomposition and the rate of CO in subsequent gasification of deposited carbons with CO_2 over Ni/TiO_2. Contact of methane with a fresh Ni/TiO_2 catalyst produced hydrogen selectively as a gaseous product. The conversion of methane at 10 min of time on stream (the first plot) was 8.8%. The formation rate of hydrogen declined with time on stream and the catalyst was deactivated completely within

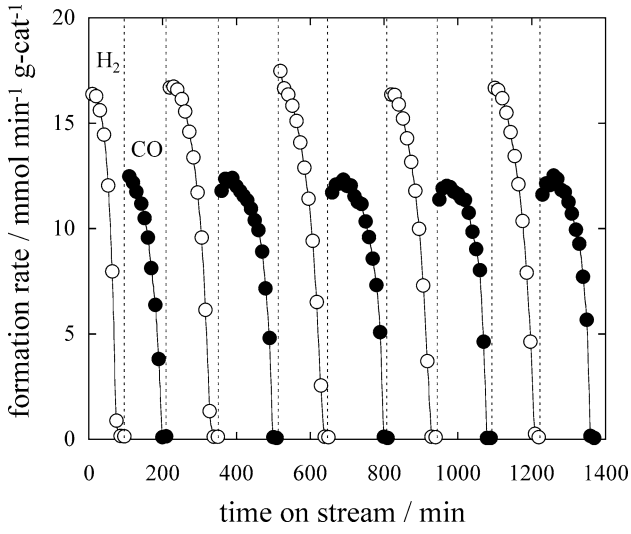

Fig. 1. Kinetic curves of the formation rate of hydrogen in methane decomposition and that of CO in subsequent gasification of deposited carbons with CO_2 over Ni/TiO_2 catalyst. Ni(2.5 wt%)/TiO_2: 0.04 g, methane decomposition; $P(CH_4) = 101.3$ kPa, 60 ml min^{-1}, gasification of deposited carbon with CO_2; $P(CO_2) = 33$ kPa, $P(Ar) = 68.3$ kPa, flow rate = 60 ml min^{-1}.

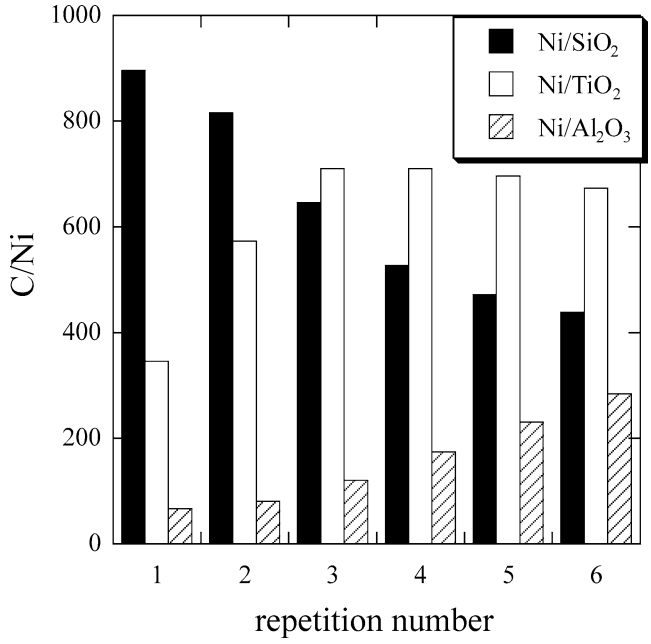

Fig. 2. Change in carbon yields (C/Ni) evaluated at the complete deactivation of each catalyst for methane decomposition as a function of the repeated number.

100 min of time on stream. The methane remaining in the reactor was flushed out with Ar and CO_2 was introduced at 923 K. The contact of CO_2 with carbons from methane formed CO efficiently from 110 to 210 min of time on stream. The carbons deposited by methane decomposition were converted into CO with a conversion higher than 95%. After the formation of CO could not be observed, CO_2 was purged out with Ar and methane was introduced at 823 K again. The contact of methane with the catalyst produced hydrogen again and a kinetic curve similar to that of the first run (0–100 min) was observed. These results indicate that gasification of deposited carbons with CO_2 results in the selective formation of CO as well as the regeneration of the deactivated catalyst for methane decomposition. As can be seen in Fig. 1, the reaction cycles of methane decomposition and subsequent gasification of deposited carbons with CO_2 could be carried out repeatedly. The reaction cycles over Ni/Al_2O_3 and Ni/SiO_2 could also be performed repeatedly (the kinetic curves are not shown). For gasification of the deposited carbons with CO_2 over all the catalysts, the carbons deposited by the previous methane decomposition were converted into CO with conversions higher than 95% irrespective of the repeated numbers. However, the change in catalytic activity for each methane decomposition with the repeated cycles was different among the three catalysts. Fig. 2 shows the change in carbon yields (C/Ni) evaluated at the complete deactivation of the catalysts for methane decomposition as a function of the repeated number. At the first methane decomposition, Ni/SiO_2 showed the highest C/Ni value among all the catalysts. However, the C/Ni value for Ni/SiO_2 decreased significantly with repeated reactions. The C/Ni value for Ni/TiO_2 increased from the first to the third cycle and became unchanged since the third cycle. As for Ni/Al_2O_3, the C/Ni value of the first methane decomposition was very low, but the value increased gradually with the repeated number.

3.2. SEM images and BEIs of the catalysts during repeated reactions

Fig. 3 shows SEM images and back-scattering electron images (BEI) of Ni/SiO_2 in the early period of methane decomposition (C/Ni = ca. 50). Each BEI was measured at the same time as the corresponding SEM image. SEM images show the preferential formation of carbon nanofibers on the Ni/SiO_2 catalyst, indicating that the carbons from methane grow with a filamentous structure. BEIs show many bright spots which indicate the position and size of Ni metal particles in this case. Most of the bright spots in the BEIs were located at the tip of carbon nanofibers and the sizes of the bright spots were almost the same as that of the corresponding carbon nanofibers. These results indicate that a Ni metal particle produces a carbon nanofiber of the same size as itself. The Ni metal adsorbs methane and decomposes it into hydrogen and carbon atom and the process is followed by diffusion of carbon atoms on the metal surface and/or through the bulk of metal particle to the precipitation sites, where they are crystallized to form a graphitic layer, starting growth of a carbon nanofiber [12]. In the BEI of the catalyst after the first methane decomposition (a), it was found that the sizes of bright spots ranged from 40 to 100 nm. On the other hand, the BEIs of the catalyst after the third and the fifth methane decomposition show some bright spots with the sizes larger than 200 nm, indicating that Ni metal particles were aggregated during the repeated reactions. It is worthwhile noting that Ni metal particles with too large

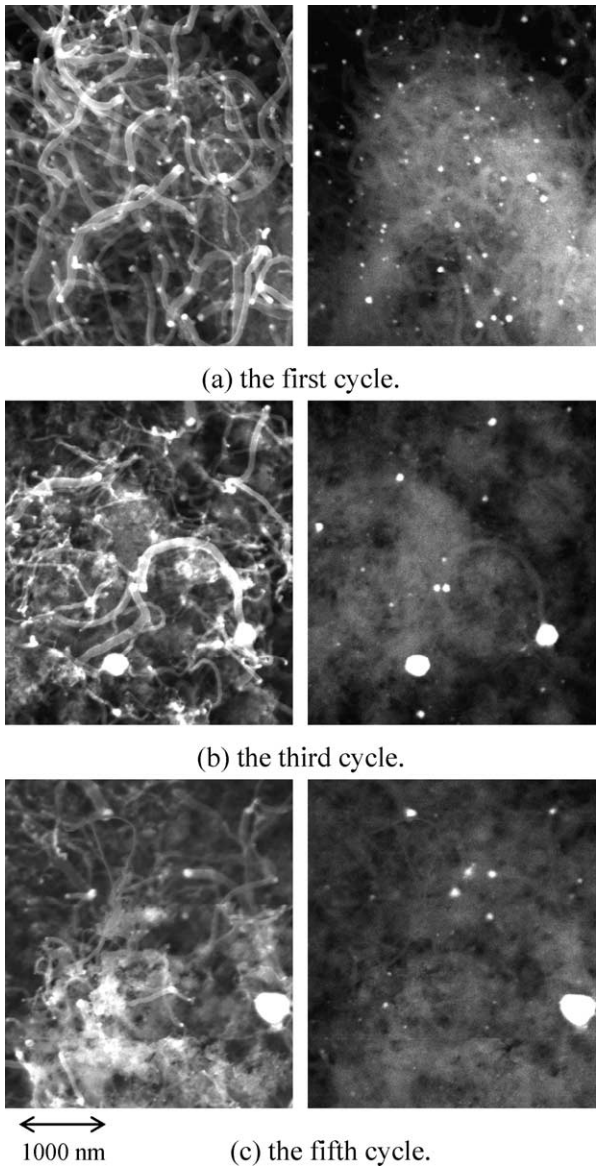

Fig. 3. SEM images (left side) and back-scattering electron images (right side) of Ni/SiO_2 catalyst in the early period of the first (a), third (b), and fifth methane decomposition (c).

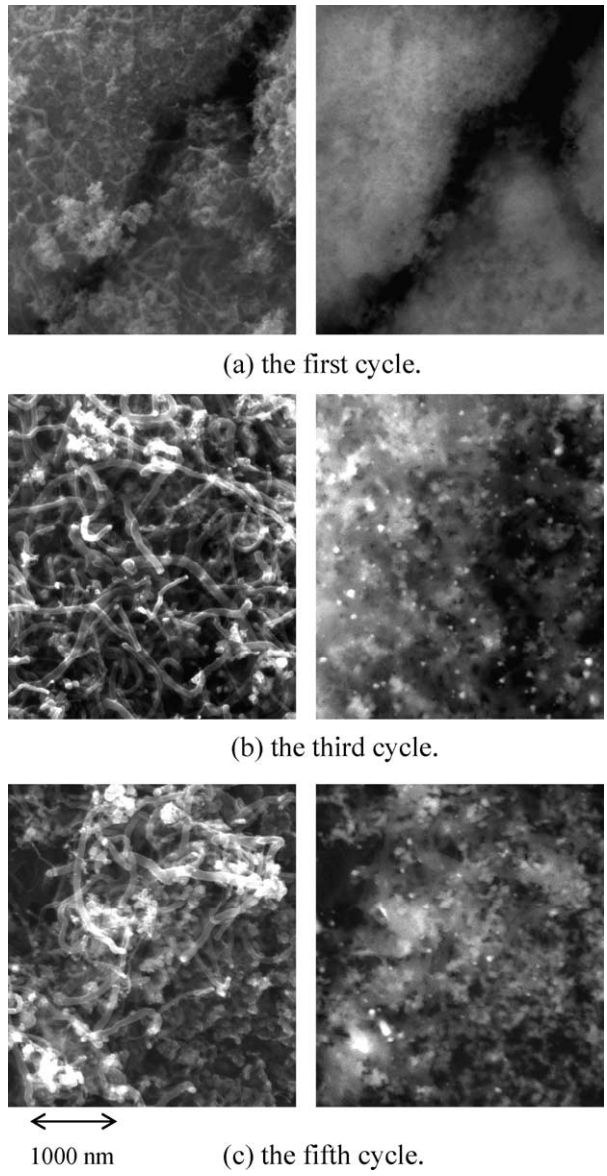

Fig. 4. SEM images (left side) and back-scattering electron images (right side) of Ni/TiO_2 catalyst in the early period of the first (a), third (b), and fifth methane decomposition (c).

sizes (> 200 nm) did not form carbon nanofibers, while the metal particles with sizes from 30 to 120 nm formed carbon nanofibers. We have already proposed that the particle size of Ni metal determines the carbon yield in methane decomposition over supported Ni catalysts; that is, Ni metal particles of the diameter range from 60 to 100 nm are the most effective ones for methane decomposition [13]. The catalytic activity of Ni/SiO_2 for the first methane decomposition was high since the fraction of Ni metal particles with diameters from 60 to 100 nm was high for the fresh Ni/SiO_2. With the repeated cycles, the Ni metal particles were aggregated, which brought about a decrease in the fraction of Ni metal particles of the effective diameter (60–100 nm). This explains the reason why Ni/SiO_2 had been deactivated for the methane decomposition with repeated reactions (Fig. 2).

Fig. 4 shows the SEM images and BEIs of Ni/TiO_2 catalyst in the early period of repeated methane decomposition (C/Ni = ca. 50). As for the catalyst after the first methane decomposition, the SEM image shows many carbon nanofibers with diameters smaller than 40 nm and the corresponding BEI shows no clear bright spot. As described earlier, the diameter of carbon nanofiber was almost the same as that of Ni metal particle on the tip of the corresponding carbon nanofiber. Therefore, the diameter of Ni metal particles on the Ni/TiO_2 in the early period of the first methane decomposition would be smaller than 40 nm. We could observe the clear bright spots in the BEI when Ni metal particles of sizes larger than 40 nm were present on the catalyst surface, as shown in Fig. 3. The unclear BEI of the Ni/TiO_2 in the early period of the first methane decom-

position may imply the presence of Ni metal particles with size below the detectable limit; i.e., the unclear image would show the presence of TiO_2. On the other hand, many carbon nanofibers with diameters of 50–100 nm were found in the SEM image of the catalyst after the third methane decomposition and many bright spots of the same size range as the carbon nanofibers were observed in the corresponding BEI image. Therefore, the small Ni metal particles must have been aggregated during the first and second cycles. However, as described earlier, the catalytic activity of Ni/TiO_2 increased with the cycles from the first to the third methane decomposition. This suggests that the aggregation of Ni metal particles in Ni/TiO_2 is desirable for improving the catalytic activity for methane decomposition, i.e., this aggregation of Ni metal results in the formation of metal particles with the diameter range effective for methane decomposition (60–100 nm). The size of carbon nanofibers and bright spots observed in the SEM image and BEI of Ni/TiO_2 after the fifth methane decomposition was almost the same as that after the third reaction. Thus, TiO_2 support prevents serious aggregation of Ni metal after the third methane decomposition and may maintain the size of Ni particles in the range favorable for the growth of carbon nanofibers, which keep the catalytic activity of Ni/TiO_2 for the methane decomposition high after the third reaction cycle in Figs. 1 and 2.

Fig. 5 shows the SEM images and BEIs of Ni/Al_2O_3 in the early period of methane decomposition. For the catalyst after the first methane decomposition, many carbon nanofibers with diameters smaller than 20 nm were found in the SEM image and no clear bright spot could be observed in the corresponding BEI. On the basis of these images, we consider that Ni metal particles with diameters smaller than 20 nm were dominant in a fresh catalyst and these metal particles produced fine carbon nanofibers. With repeated reaction cycles, the diameter range of carbon nanofibers became larger. In addition, the bright spots with diameter ranging from 40 to 60 nm could be observed in the BEIs of the catalyst after the third and the fifth methane decomposition, although the number of spots was very few. These results suggest that Ni metal particles smaller than 20 nm are aggregated into ones ranging from 40 to 60 nm with repeated reaction cycles. However, the size range of carbon nanofibers and bright spots was very small even after the fifth methane decomposition, which indicates that the aggregation of Ni metal particles with repeated cycles is not fast for Ni/Al_2O_3. As described earlier, the catalytic activity of Ni/Al_2O_3 for methane decomposition increased with the repeated number. This improvement in catalytic activity must have resulted from the change in the particle size; i.e., the diameter range of Ni metal particles is too small to be effective for methane decomposition in the early cycles, whereas the particle size range approaches the ones that are effective for methane decomposition (60–100 nm) by the repeated reactions, which increase the catalytic activity of Ni/Al_2O_3 for methane decomposition.

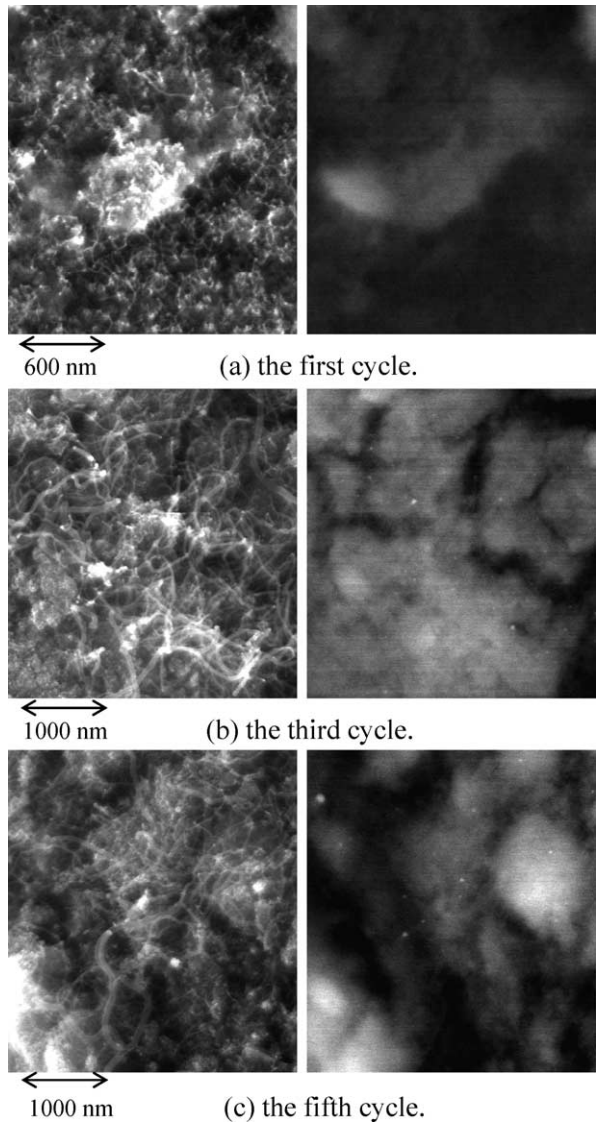

Fig. 5. SEM images (left side) and back-scattering electron images (right side) of Ni/Al_2O_3 catalyst in the early period of the first (a), third (b), and fifth methane decomposition (c).

3.3. Ni K-edge XANES/EXAFS of the catalysts during repeated cycles

Fig. 6 shows Ni K-edge XANES spectra of Ni/SiO_2 catalyst at the different stages of the repeated reactions and of Ni foil. The XANES spectra of Ni/TiO_2 are shown in Fig. 7. The XANES spectra of fresh Ni/SiO_2 and Ni/TiO_2 resemble that of a Ni foil, indicating that Ni species in the fresh catalysts are present in the state of Ni metal mainly. In addition, the XANES spectra of Ni/SiO_2 and Ni/TiO_2 in the early period of methane decomposition, (c)–(e), were similar to those of the corresponding fresh catalyst (b) irrespective of the repeated number of reactions, indicating that the Ni species in the active catalysts for methane decomposition is present as a Ni metal crystallite. In contrast, deactivation of both catalysts for methane decomposition

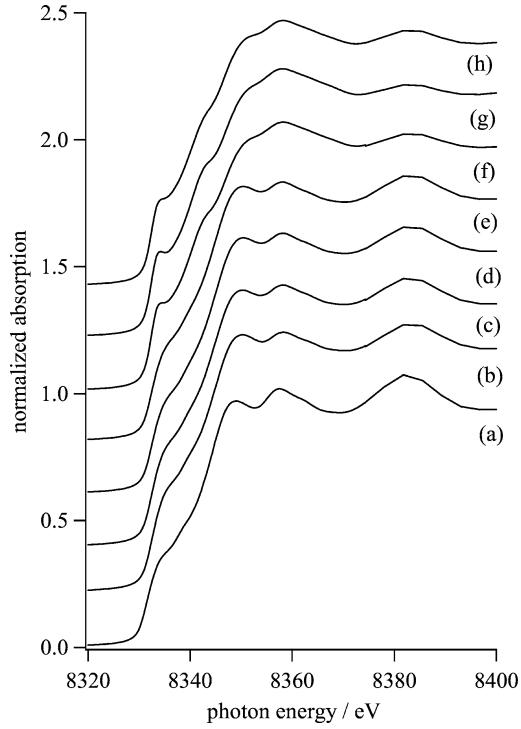

Fig. 6. Ni K-edge XANES spectra of Ni/SiO_2 catalyst and Ni foil. (a) Ni foil; (b) fresh catalyst (after reduction with hydrogen); (c), (d), and (e) in the early period of methane decomposition of the first, third, and fifth cycle; (f), (g), and (h) after complete deactivation for methane decomposition of the first, third, and fifth cycle.

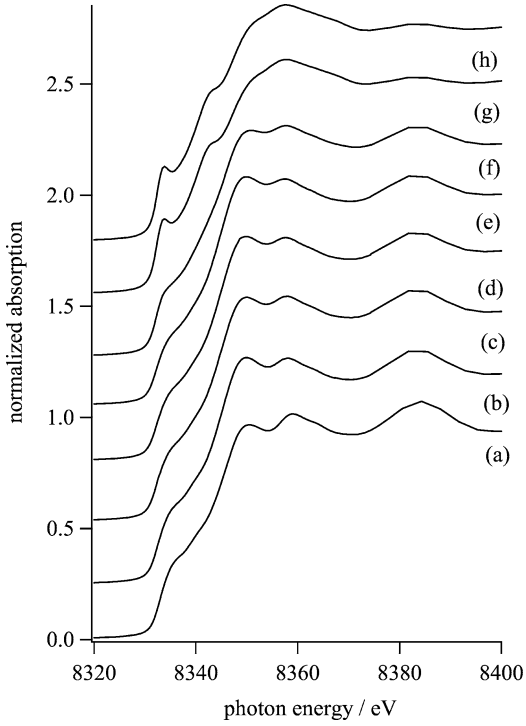

Fig. 7. Ni K-edge XANES spectra of Ni/TiO_2 catalyst and Ni foil. (a) Ni foil; (b) fresh catalyst (after reduction with hydrogen); (c), (d), and (e) in the early period of the methane decomposition of the first, third, and fifth cycle; (f), (g), and (h) after complete deactivation for methane decomposition of the first, third, and fifth cycle.

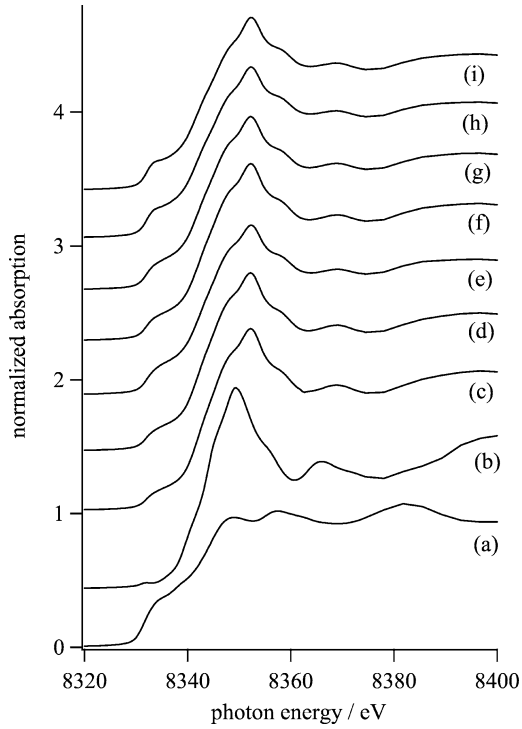

Fig. 8. Ni K-edge XANES spectra of Ni/Al_2O_3 catalyst, Ni foil, and NiO. (a) Ni foil; (b) NiO; (c) fresh catalyst (after reduction with hydrogen); (d), (e), and (f) in the early period of methane decomposition of the first, third, and fifth cycle; (g), (h), and (i), after complete deactivation for methane decomposition of the first, third, and fifth cycle.

brought about the change in XANES spectra, (f)–(h); i.e., the two shoulder peaks were observed at 8332 and 8341 eV and two peaks at 8349 and 8358 eV characteristic of Ni metal became faint. We have already reported that the change in the XANES spectrum during the deactivation of the catalyst for methane decomposition can be assigned to the structural change of the Ni species from Ni metal to some nickel carbide species [14]. Thus, some parts of Ni metal particles present at the tips of carbon nanofibers change into nickel carbide species at the deactivation of Ni/SiO_2 and Ni/TiO_2.

Fig. 8 shows Ni K-edge XANES spectra of Ni/Al_2O_3 at different stages of the repeated reactions. XANES spectra of Ni foil (a) and NiO (b) are also shown in Fig. 8. The features of the XANES spectrum of NiO are significantly different from those of Ni foil; i.e., threshold is observed at ca. 8330 eV for the XANES spectrum of a Ni foil and sharp absorption is observed at ca. 8350 eV for that of NiO. The XANES spectrum of fresh Ni/Al_2O_3 (c) was similar to that of NiO rather than that of Ni foil, although a threshold at 8330 eV, which is characteristic of the spectrum of Ni foil, could be seen in the spectrum of a fresh catalyst. Thus, Ni species in fresh Ni/Al_2O_3 consist of Ni metal and Ni(II) species that is surrounded by oxygen atoms. As will be described later, the XRD pattern of fresh Ni/Al_2O_3 showed the presence of $NiAl_2O_4$. Therefore, the Ni(II) species observed by XANES would be attributed to the presence of $NiAl_2O_4$. XANES spectra of Ni/Al_2O_3 in

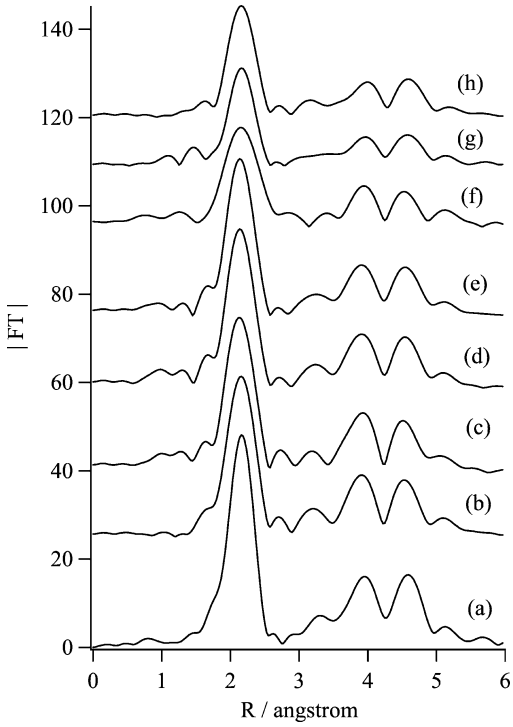

Fig. 9. Fourier transforms of k^3-weighted Ni K-edge EXAFS of Ni/SiO_2 catalyst and Ni foil. (a) Ni foil; (b) fresh catalyst (after reduction with hydrogen); (c), (d), and (e), in the early period of methane decomposition of the first, third, and fifth cycle; (f), (g), and (h), after complete deactivation for methane decomposition of the first, third, and fifth cycle.

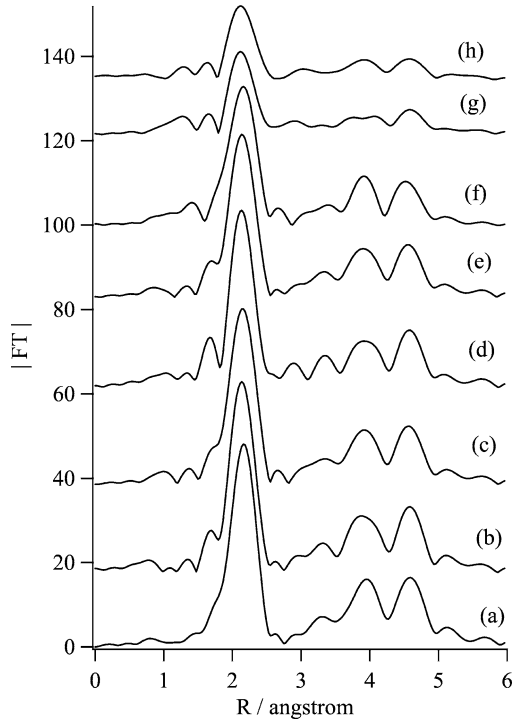

Fig. 10. Fourier transforms of k^3-weighted Ni K-edge EXAFS of Ni/TiO_2 catalyst and Ni foil. (a) Ni foil; (b) fresh catalyst (after reduction with hydrogen); (c), (d), and (e), in the early period of methane decomposition of the first, third, and fifth cycle; (f), (g), and (h), after complete deactivation for methane decomposition of the first, third, and fifth cycle.

the early period of methane decomposition ((d), (e), and (f)) were similar to those of a fresh one. However, the threshold at 8330 eV became slightly intense and absorption at 8350 eV became weak with the repeated cycles. These results suggested that the fraction of Ni metal to all Ni species in Ni/Al_2O_3 became greater with repeated cycles. It is likely that a part of $NiAl_2O_4$ in Ni/Al_2O_3 changes into Ni metal during the repeated cycles because carbon and hydrogen formed by methane decomposition could work as reductants for $NiAl_2O_4$, as demonstrated in the case of the steam reforming of methane over supported Ni catalyst [15].

Fig. 9 shows Fourier transforms (RSF; radial structure function) of k^3-weighted Ni K-edge EXAFS of Ni/SiO_2 at different stages of the repeated reactions and Ni foil. The results for Ni/TiO_2 are shown in Fig. 10. The RSFs of fresh Ni/SiO_2 and Ni/TiO_2 (b) were similar to that of Ni foil (a), which was consistent with the XANES spectra. The peak intensities around 2.2 Å due to Ni–Ni for both the catalysts in the early period of methane decomposition (spectra (c)–(e)) did not change irrespective of the number of repeated reactions. The peak intensity corresponds to an average size of Ni metal crystallite. Thus, the average crystallite size of Ni metal in the active Ni/SiO_2 and Ni/TiO_2 (in the early period of methane decomposition) does not change by repeated reactions. As described earlier, the increase in the particle size of Ni metal was observed by the SEM images of Ni/SiO_2 during the repeated reactions and of Ni/TiO_2 in the early cycles. Taking the results of the EXAFS and the SEM images for both the catalysts into consideration, we consider that the aggregation of Ni metal particles during the repeated reactions is not accompanied by an increase in the crystallite size of Ni metal.

On the other hand, the peaks due to Ni–Ni in RSFs of both deactivated catalysts ((f), (g), and (h)) were low and broad, compared to those in the active catalysts ((c), (d), and (e)). The XANES spectra (Figs. 6 and 7) showed the formation of Ni carbide species after the deactivation of the catalysts for methane decomposition. The weakening and broadening of the peak due to Ni–Ni in RSFs of the deactivated catalysts can be ascribed to the interference by carbon in the environments of Ni–Ni bonds due to the formation of nickel carbide species for the deactivated catalysts [14].

Fig. 11 shows Fourier transforms of k^3-weighted Ni K-edge EXAFS (RSFs) of Ni/Al_2O_3 catalyst, Ni foil, and NiO. RSF of fresh Ni/Al_2O_3 (spectrum (c)) showed two peaks at 1.4 and 2.1 Å. Taking into consideration the results drawn by the XANES spectra that some Ni species are surrounded by oxygen atoms, the former peak could be assigned to a Ni–O bond. The Ni species would be $NiAl_2O_4$ based on the XRD pattern of Ni/Al_2O_3. The position of the latter peak (at 2.1 Å) in RSF for fresh Ni/Al_2O_3 was close to that for Ni foil (2.2 Å) rather than that for NiO (2.8 Å). On the basis of the EXAFS and XANES spectra, we consider that Ni species in fresh Ni/Al_2O_3 consist of Ni metal and $NiAl_2O_4$.

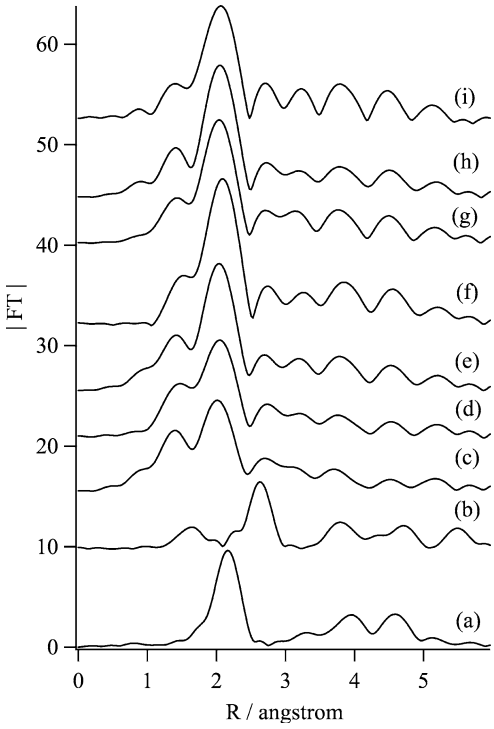

Fig. 11. Fourier transforms of k^3-weighted Ni K-edge EXAFS of Ni/Al_2O_3 catalyst, Ni foil, and NiO. (a) Ni foil; (b) NiO; (c) fresh catalyst (after reduction with hydrogen); (d), (e), and (f), in the early period of methane decomposition of the first, third, and fifth cycle; (g), (h), and (i), after complete deactivation for methane decomposition of the first, third, and fifth cycle. Magnitudes for Fourier transforms of Ni foil and NiO were divided by 5.

RSFs for Ni/Al_2O_3 in the early period of methane decomposition also showed the two peaks due to Ni–O and Ni–Ni irrespective of the number of repeated reactions. However, the intensity of the peak due to Ni–O became lower and that of the peak due to Ni–Ni became higher with the repeated cycles. These changes in RSFs would be assigned to the reduction of a part of $NiAl_2O_4$ to Ni metal. In addition to the aggregation of small Ni metal particles observed by the SEM images, the reduction of Ni(II) species into Ni metal with the repeated reactions should bring about improvement in the catalytic activity of Ni/Al_2O_3 for methane decomposition because the reduction increases the total number of active sites (Ni metal). On the other hand, the peak due to Ni–Ni in the RSFs of Ni/Al_2O_3 deactivated for the first and third methane decomposition became intense compared to that in the early period of the corresponding methane decomposition, suggesting that the fraction of Ni metal to all the Ni species increased during methane decomposition. Thus, the reduction of Ni(II) species into Ni metal would take place during methane decomposition.

3.4. Role of catalytic supports

Finally, we would discuss the role of catalytic supports in the structural change of Ni species during the repeated cycles. Fig. 12 shows SEM images and BEIs of

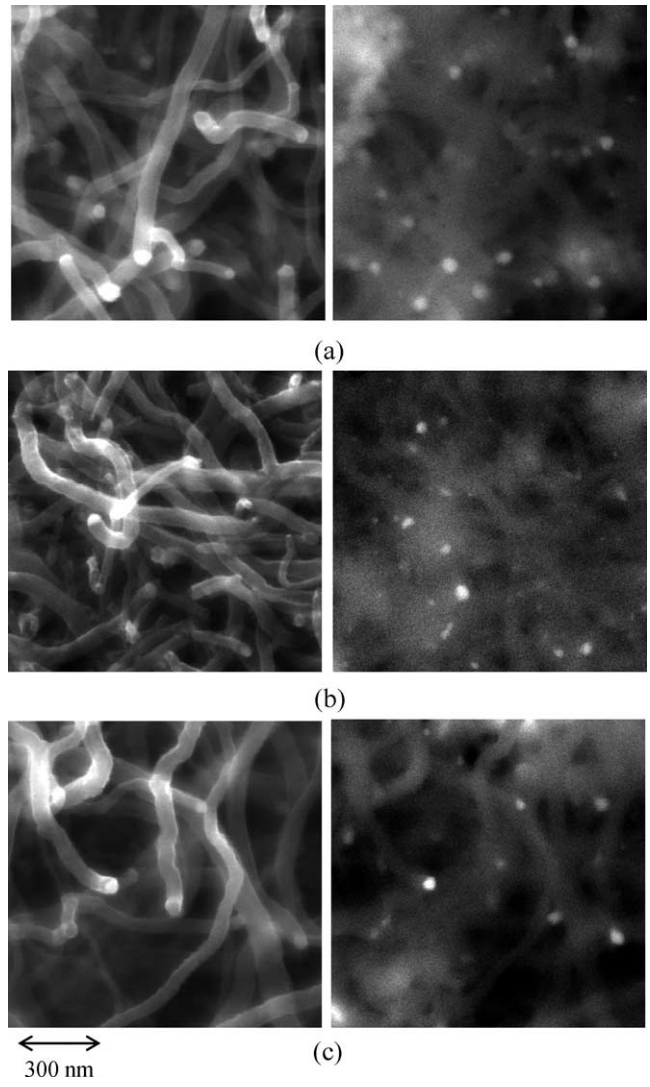

Fig. 12. SEM images and back-scattering electron images of Ni(10 wt%)/TiO_2 catalyst before and after gasification of carbon nanofibers with CO_2. (a) After methane decomposition (C/Ni = 200); (b) and (c), the carbons were gasified with CO_2 from C/Ni = 200 to 150 and 100, respectively.

Ni (10 wt%)/TiO_2 before and after gasification of carbon nanofibers with CO_2. After the carbons of C/Ni = 200 were deposited on Ni/TiO_2 by methane decomposition, the carbons were gasified with CO_2 to C/Ni = 150 (b) and 100 (c). To examine the interaction of Ni metal particles with carbon nanofibers, Ni/TiO_2 with a relatively high Ni loading, i.e., Ni (10 wt%)/TiO_2 instead of Ni (2.5 wt%)/TiO_2, was utilized for the measurement. In the SEM image of the catalyst after methane decomposition (a), carbon nanofibers with diameters from 60 to 100 nm were found and a Ni metal particle was observed at the tip of each carbon nanofiber in the corresponding BEI image. SEM images and BEIs of the catalyst after the gasification of carbon nanofibers with CO_2 showed that most of the Ni metal particles were also present at the tip of carbon nanofibers. In addition, we have already demonstrated that the carbon nanofibers which had been washed with aqueous HNO_3 to remove Ni species were

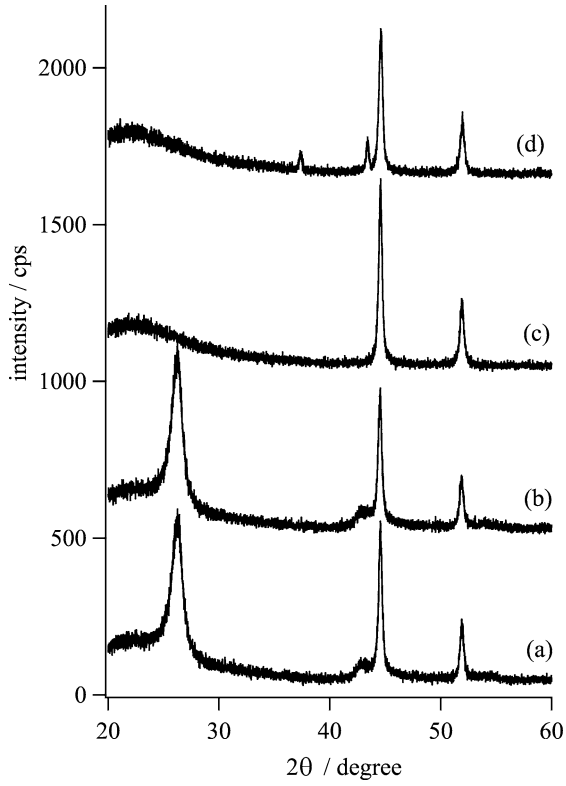

Fig. 13. XRD patterns of Ni(10 wt%)/SiO_2 catalyst before and after gasification of carbon nanofibers with CO_2. (a) After methane decomposition (C/Ni = 50); (b), (c), and (d), carbons were gasified with CO_2 from C/Ni = 50 to 40, 2, and 0, respectively.

not gasified with CO_2 at 923 K [9]. Therefore, we consider that the Ni metal particle at the tip of a carbon nanofiber catalyzes the gasification of the contacted carbon with CO_2 to shorten the length of the fiber.

Fig. 13 shows XRD patterns of Ni (10 wt%)/SiO_2 before and after the gasification of carbon nanofibers with CO_2. To obtain intense diffraction lines due to Ni species, a silica support was utilized and the loading amount of Ni was adjusted to be 10 wt% since the diffraction line due to silica is not overlapped with that of Ni species due to the amorphous structure of silica. After the carbons corresponding to the amount of C/Ni = 50 were deposited on the Ni/SiO_2 by methane decomposition, they were gasified with CO_2 to C/Ni = 40, 2, and 0. The XRD pattern of Ni/SiO_2 after methane decomposition (a) showed the diffraction lines due to Ni metal crystallite at $2\theta = 44$ and 52° and due to deposited carbons at $2\theta = 26$ and 43°. The diffraction lines due to deposited carbons disappeared upon gasification with CO_2. After complete gasification of deposited carbons (d), diffraction lines due to NiO appeared at $2\theta = 37.5$ and 43.5° in addition to those due to Ni metal. The results suggest that Ni metal particles are oxidized gradually with CO_2 after the complete gasification of deposited carbons, while Ni species are preserved as Ni metal during gasification when the deposited carbons remain on the catalyst [16]. It is likely that Ni species are present as Ni metal during gasification because the carbon nanofibers work as reductants for Ni species.

As described earlier, most Ni metal particles are present at the tip of carbon nanofibers during methane decomposition and the gasification of carbon nanofibers with CO_2. The Ni metal particles during the reactions are spatially apart from each other because they are located on the tip of carbon nanofibers. Thus, the contact between the Ni metal particles, i.e., the aggregation of them, would not take place during the reactions. However, when carbon nanofibers are gasified completely, Ni metal particles inevitably return to the supports. These Ni metal particles on the supports would be oxidized partially to NiO with CO_2 as demonstrated in Fig. 13. If the interaction between the Ni species and catalytic supports is weak, the nickel species (Ni metal and/or NiO) migrate on the supports to be aggregated when they return to the surface of the support.

Here, we speculate that the important point for the suppression of aggregation of Ni species during the repeated reactions is how strong is the interaction of the supports with Ni metal particles or with those partially oxidized by CO_2. Fig. 14 shows XRD patterns of oxidized Ni/SiO_2, Ni/TiO_2, and Ni/Al_2O_3. To obtain intense diffraction lines, the loading amount of Ni increased for Ni/TiO_2 and Ni/Al_2O_3. For the XRD pattern of oxidized Ni/SiO_2 (a), diffraction

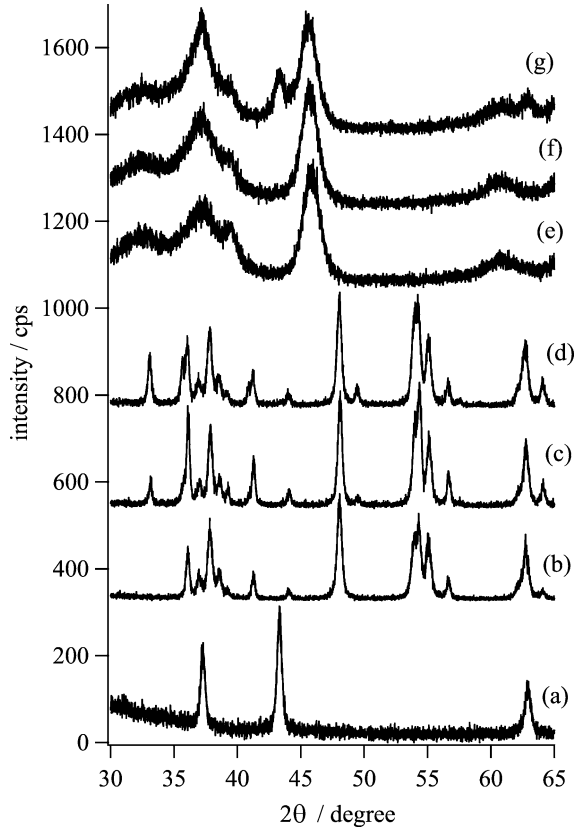

Fig. 14. XRD patterns of oxidized Ni catalysts and catalytic supports. (a) Ni(5 wt%)/SiO_2; (b) TiO_2 (JRC-TIO4); (c) Ni(2.5 wt%)/TiO_2; (d) Ni (5 wt%)/TiO_2; (e) Al_2O_3 (JRC-ALO4); (f) Ni(5 wt%)/Al_2O_3; (g) Ni (10 wt%)/Al_2O_3.

lines due to NiO were found at $2\theta = 37.5$, 43.5, and 63°. On the other hand, diffraction lines due to $NiTiO_3$ and $NiAl_2O_4$ were observed at $2\theta = 33$ and 49° and at $2\theta = 37$ and 46° in the XRD patterns of oxidized Ni/TiO_2 and Ni/Al_2O_3, respectively, although the diffraction lines due to $NiAl_2O_4$ were overlapped with those due to Al_2O_3 [17, 18]. It is unlikely that the compound oxides ($NiTiO_3$ and $NiAl_2O_4$) would migrate preferentially on the catalytic supports [19–21], compared to NiO on silica, which prevent the serious aggregation of Ni species on Ni/Al_2O_3 and Ni/TiO_2 during the repeated reactions as described earlier (Figs. 4 and 5). This is the reason why the catalytic activities of Ni/TiO_2 and Ni/Al_2O_3 for methane decomposition did not decrease with repeated cycles.

4. Conclusions

We conclude as follows from the results mentioned previously:

1. Ni species in fresh Ni/SiO_2 were present as Ni metal particles of diameter from 40 to 100 nm. The Ni metal particles were aggregated gradually with repeated reactions to form ones larger than 200 nm, which were inactive for methane decomposition. This aggregation brought about the deactivation of Ni/SiO_2 for methane decomposition.
2. Ni species in fresh Ni/TiO_2 were present as Ni metal particles with diameter of ca. 40 nm. With repeated reactions, the Ni metal particles were aggregated and the diameter of the metal particles approached the optimum one for methane decomposition (60–100 nm). However, TiO_2 support prevented the serious aggregation of Ni metal particles. Thus, the catalytic activity of Ni/TiO_2 for methane decomposition was kept high during the repeated reactions.
3. Ni species in fresh Ni/Al_2O_3 were composed of $NiAl_2O_4$ and Ni metal particles of diameter smaller than 20 nm. $NiAl_2O_4$ was gradually reduced into Ni metal. The formed Ni metal was aggregated gradually, which brought about increases in the number and the size of Ni metal particles active for methane decomposition. Thus, the catalytic activity of Ni/Al_2O_3 for methane decomposition increased gradually during repeated reactions.

References

[1] Anonymous, Chem. Eng. 69 (1962) 90.
[2] N.Z. Muradov, Int. J. Hydrogen. Energy 18 (1993) 211.
[3] T. Ishihara, Y. Miyashita, H. Iseda, Y. Takita, Chem. Lett. (1995) 93.
[4] T.V. Choudhary, C. Sivadinarayana, C.C. Chusuei, A. Klinghoffer, D.W. Goodman, J. Catal. 199 (2001) 9.
[5] K. Otsuka, S. Kobayashi, S. Takenaka, Appl. Catal. A 190 (2000) 261.
[6] S.K. Shiakhutdinov, L.B. Avdeeva, O.V. Goncharova, D.I. Kochubey, B.N. Novgorodov, L.M. Plyasova, Appl. Catal. A 126 (1995) 125.
[7] M.A. Ermakova, D.Yu. Ermakov, G.G. Kuvshinov, L.M. Plyasova, J. Catal. 187 (1999) 77.
[8] S. Takenaka, H. Ogihara, I. Yamanaka, K. Otsuka, Appl. Catal. A 217 (2001) 101.
[9] S. Takenaka, K. Otsuka, Chem. Lett. (2001) 218.
[10] S. Takenaka, Y. Tomikubo, E. Kato, K. Otsuka, Fuel, in press.
[11] S. Yoshida, S. Takenaka, T. Tanaka, H. Hirano, H. Hayashi, Stud. Surf. Sci. Catal. 101 (1996) 871.
[12] R.T.K. Baker, Carbon 27 (1989) 315.
[13] S. Takenaka, S. Kobayashi, H. Ogihara, K. Otsuka, J. Catal. 217 (2003) 79.
[14] S. Takenaka, H. Ogihara, K. Otsuka, J. Catal. 208 (2002) 54.
[15] K. Tomishige, Y.G. Chen, K. Fujimoto, J. Catal. 181 (1999) 91.
[16] V.Yu. Bychkov, O.V. Krylov, V.N. Korchak, Kinet. Catal. 43 (2002) 86.
[17] G.R. Rao, C.N.R. Rao, J. Phys. Chem. 94 (1990) 7986.
[18] Y.J. Haung, J.A. Schwarz, J.R. Diehl, J.P. Baltrus, Appl. Catal. 36 (1988) 163.
[19] T. Arunarkavalli, G.U. Kulkarni, G. Sankar, C.N.R. Rao, Catal. Lett. 17 (1993) 29.
[20] Z. Xu, Y. Li, J. Zhang, L. Chang, R. Zhou, Z. Duan, Appl. Catal. A 210 (2001) 45.
[21] J.M. Jehng, C.M. Chen, Catal. Lett. 77 (2001) 147.